Evidence of hot and cold spots on the Fermi surface of LiFeAs

J. Fink,[1,2,3] J. Nayak,[2] E. D. L. Rienks,[1,3] J. Bannies,[2] S. Wurmehl,[1,3] S. Aswartham,[1] I. Morozov,[1] R. Kappenberger,[1] M. A. ElGhazali,[2,3] L. Craco,[1,4] H. Rosner,[2] C. Felser,[2] and B. Büchner[1,3]

[1]*Leibniz Institute for Solid State and Materials Research Dresden, Helmholtzstr. 20, D-01069 Dresden, Germany*

[2]*Max Planck Institute for Chemical Physics of Solids, D-01187 Dresden, Germany*

[3]*Institut für Festkörperphysik, Technische Universität Dresden, D-01062 Dresden, Germany*

[4]*Instituto de Fisica, Universidade Federal de Mato Grosso, 78060-900 Cuiabá, MT, Brazil*

(Received 27 July 2018; revised manuscript received 24 May 2019; published 28 June 2019)

Angle-resolved photoemission spectroscopy (ARPES) is used to study the energy and momentum dependence of the inelastic scattering rates and the mass renormalization of charge carriers in LiFeAs at several high symmetry points in the Brillouin zone. A strong and linear-in-energy scattering rate is observed for sections of the Fermi surface having predominantly Fe $3d_{xy/yz}$ orbital character on the inner hole and on electron pockets. We assign them to hot spots with marginal Fermi liquid character inducing high antiferromagnetic and pairing susceptibilities. The outer hole pocket, with Fe $3d_{xy}$ orbital character, has a reduced but still linear in energy scattering rate. Finally, we assign sections on the middle hole pockets with Fe $3d_{xz,yz}$ orbital character and on the electron pockets with Fe $3d_{xy}$ orbital character to cold spots because there we observe a quadratic-in-energy scattering rate with Fermi-liquid behavior. These cold spots prevail the transport properties. Our results indicate a strong *momentum* dependence of the scattering rates. We also have indications that the scattering rates in correlated systems are fundamentally different from those in noncorrelated materials because in the former the Pauli principle is not operative. We compare our results for the scattering rates with combined density functional plus dynamical mean-field theory calculations. The work provides a generic microscopic understanding of macroscopic properties of multiorbital unconventional superconductors.

DOI: 10.1103/PhysRevB.99.245156

I. INTRODUCTION

Since the discovery of iron-based superconductors (FeSCs) [1] there is an ongoing debate about whether their electronic structure is more itinerant or localized [2]. Transport properties and optical spectroscopy indicate predominantly a Fermi liquid behavior [3–5]. On the other hand, high-T_c $s^{\pm}$ superconductivity and antiferromagnetism are believed to occur due to strong correlation enhanced scattering of the charge carriers between hole and electron pockets [6]. In these multiorbital systems, it is likely that the different properties are related to the intrinsic multiorbital nature of electron and hole pockets. This is supported by combined density functional plus dynamical mean field theory (DFT+DMFT) calculations, which pointed out that the strength of correlation effects strongly depends on the orbital character of the bands due to their different respective filling [7–13] and that for half-filled orbitals, correlation effects are not only determined by the onsite Coulomb interaction but also by Hund's exchange interaction.

The strength of correlation effects, however, may be determined not only by the orbital character of the bands but also by the nesting conditions and, thus, by the momentum [14,15]. In order to obtain a microscopic understanding of these effects, momentum dependent information on the character of the states near the Fermi level (E_F) is necessary. Angle-resolved photoemission spectroscopy (ARPES) is a suitable method to obtain this momentum dependent information because it provides the energy (E) and momentum ($\mathbf{k}$) dependent scattering rates Γ or lifetimes $\tau = \hbar/\Gamma$ of the charge carriers [16] which are related to the imaginary part of the self-energy $\Im\Sigma$ by $\Gamma = -2Z\Im\Sigma$, where $Z = m_b/m^* = \frac{1}{1-\frac{\partial\Re\Sigma}{\partial E}}$ is the quasiparticle residue and m^*/m_b is the mass renormalization [17]. The latter is derived from a comparison of the ARPES data with DFT calculations. Here, we use ARPES to study the scattering rate of superconducting LiFeAs [18] in its normal state. This tetragonal compound without dopant atoms to induce disorder is particularly suited for ARPES studies [19–21].

There are numerous ARPES studies on LiFeAs [22–29]. In the investigations of the scattering rates, one of the main results was that Γ depends on the orbital character rather than on the position on the Fermi surface. This result was possibly biased by DFT+DMFT calculations on FeSCs [30,31] which are based on a local, not momentum dependent approximation for the correlation effects. The present high resolution ARPES data together with a new evaluation method comes to a different conclusion: The inelastic scattering rates depend predominantly on the momentum and only indirectly on the orbital character. Our study yields information on the location of hot (large Γ) and cold (small Γ) spots within the Brillouin zone (BZ). This will improve our microscopic understanding of the magnetic and superconducting susceptibilities (determined by the hot spots) and normal state transport properties (determined by the cold spots).

II. EXPERIMENTAL

LiFeAs ($T_c = 17$ K) single crystals were grown using the self-flux technique [32]. ARPES measurements

were conducted at the 1^2 and 1^3-ARPES end stations attached to the beamline UE112 PGM at BESSY, equipped with Scienta R8000 and Scienta R4000 energy analyzers, respectively. All data presented in this contribution were taken in the normal state at temperatures between 20 and 35 K. The achieved energy and angle resolutions were between 4 and 15 meV and 0.2°, respectively. Polarized photons with energies $h\nu = 20$–130 eV were employed to reach different k_z values in the BZ and spectral weight with a specific orbital character [33,34]. An inner potential of 12 eV was used to calculate the k_z values from the photon energy [35].

III. DATA EVALUATION

ARPES measures the energy and momentum dependent spectral function $A(E, \mathbf{k})$ multiplied by a transition matrix element and the Fermi function and convoluted with the energy and momentum resolution [16]. The spectral function is given by

$$A(E, \mathbf{k}) = \frac{1}{\pi} \frac{\frac{\Gamma(E,\mathbf{k})}{2}}{[E - \epsilon^*_{\mathbf{k}}]^2 + \left[\frac{\Gamma(E,\mathbf{k})}{2}\right]^2}, \quad (1)$$

where the renormalized particle energy is $\epsilon^*_{\mathbf{k}} = \epsilon_{\mathbf{k}} - \Re\Sigma(E, \mathbf{k})$. Here ϵ_k is the bare particle energy. Strictly speaking the formula for the spectral function is only valid near the Fermi level and for a small self-energy independent of momentum [17]. In this case the spectral function at constant momentum has a maximum at ϵ^*_k and a full width at half maximum of Γ. Very often the description of the spectral function is extended to higher energies [36,37].

The direct evaluation of the lifetime broadening from fits of cuts at constant momentum is difficult for highly correlated systems because $\Gamma(E)$ is strongly energy dependent and therefore such a cut is no more a Lorentzian. Usually, in ARPES the scattering rates are derived from the momentum width of the spectral weight at constant energy [37]. The lifetime broadening in energy space is obtained by multiplying the momentum width by the velocity. This works well for a linear dispersion because in this case the velocity $v(E)$ is constant in energy and therefore the contribution from the elastic scattering is constant. It is also possible to evaluate the inelastic lifetime broadening from a parabolic dispersion but then one has to take into account the energy dependence of the velocity. At the top of a hole pocket or the bottom of an electron pocket the velocity is zero and therefore this method does not work at these energies.

Therefore we have analyzed our spectra by a multivariate fit of the spectra measured in the two-dimensional $E - k$ space. We multiply the spectral function with the Fermi function and convolute it with the energy and momentum resolution. The following parameters were derived: the energy dependent lifetime broadening $\Gamma(E)$ for all measured energies, a constant slightly asymmetric amplitude, values determining the dispersion, and values determining the slightly energy and momentum dependent background.

In this way we obtain the energy dependent total scattering rate $\Gamma_t(E)$ which is the sum of the elastic scattering rate $\Gamma_e(E)$ and the inelastic scattering rate $\Gamma_i(E)$. In highly correlated systems the latter is predominantly due to electron-electron interaction. To derive $\Gamma_i(E)$ one has to subtract the elastic from the total scattering rates. In the Supplemental Material [38] we describe in detail the method which we use to subtract the energy dependent elastic scattering rates in the case of parabolic bands.

IV. THEORY

We performed density functional band structure calculations within the local density approximation including spin orbit coupling, using experimental structural parameters [18] and the full-potential local-orbital code FPLO [39] (version fplo18.00-52) with the Perdew-Wang exchange correlation potential [40]. Similar to earlier DFT+DMFT studies [41,42], the local self-energies due to the correlated Fe $3d$ problem, intrinsic to Fe-based superconductors are obtained with the multiorbital iterated perturbation theory as impurity solver [43], where $U = 2.5$ eV and $J_H = 0.7$ eV are used.

From a parabolic fit to the ARPES data and to the DFT results close to E_F we derive the renormalized mass m^* and the bare particle mass m_b, respectively. The ratio m^*/m_b yields the mass renormalizations.

V. RESULTS

In Fig. 1(a) we present a schematic Fermi surface of typical ferropnictides in a selected region in reciprocal space in the $k_z = 0$ plane. In LiFeAs for $k_z = 0$, no inner hole pocket is visible in the Fermi surface because it is about 12 meV below E_F. Using thick black solid lines we mark two cuts (I and II) along which we have performed ARPES measurements. In Figs. 1(b)–1(f) we show energy-momentum distribution maps of hole and electron pockets, recorded along cut I and cut II using different photon polarizations to select bands with different orbital character [33]. To demonstrate the existence of spectral weight with yz orbital character at E_F due to a correlation induced broadening of the band, we show a zoom in of Fig. 1(b) in Fig. 1(c). In Figs. 1(b)–1(f) we have added the dispersions calculated by DFT and DFT+DMFT. Using other photon energies, we have collected analogous data of the spectral weight in planes corresponding to $k_z = \pi/c$.

As described in Sec. III we have evaluated the ARPES data by a multivariate fit. Waterfall plots of these fits for the five points illustrated in Fig. 1(a) are presented in Fig. 2. In nearly all cases the fits are rather good. For the inner electron pocket [Fig. 2(e)] the fit is less perfect probably due to small contributions to the spectral weight from the outer hole pocket.

After subtraction of $\Gamma_e(E)$ we obtain $\Gamma_i(E)$ which is presented in Fig. 3 for the five points in the BZ (see inset). In Fig. 3 we also compare $\Gamma_i(E)$ from ARPES with DFT+DMFT results. As shown previously for the inner and outer hole pocket in other ferropnictides [44], for all points the theoretical values are considerably smaller than the experimental data. In the analyzed energy regions, the data for points (1), (3), and (5) can be well fitted by a linear relationship $\Gamma = \beta E$. At points (2) and (4) Γ_i can be fitted by a quadratic relationship $\Gamma = \gamma E^2$. We have not found a clear indication of significant electron-phonon coupling which would result in a step in $\Gamma_i(E)$ and a kink in the dispersion near the

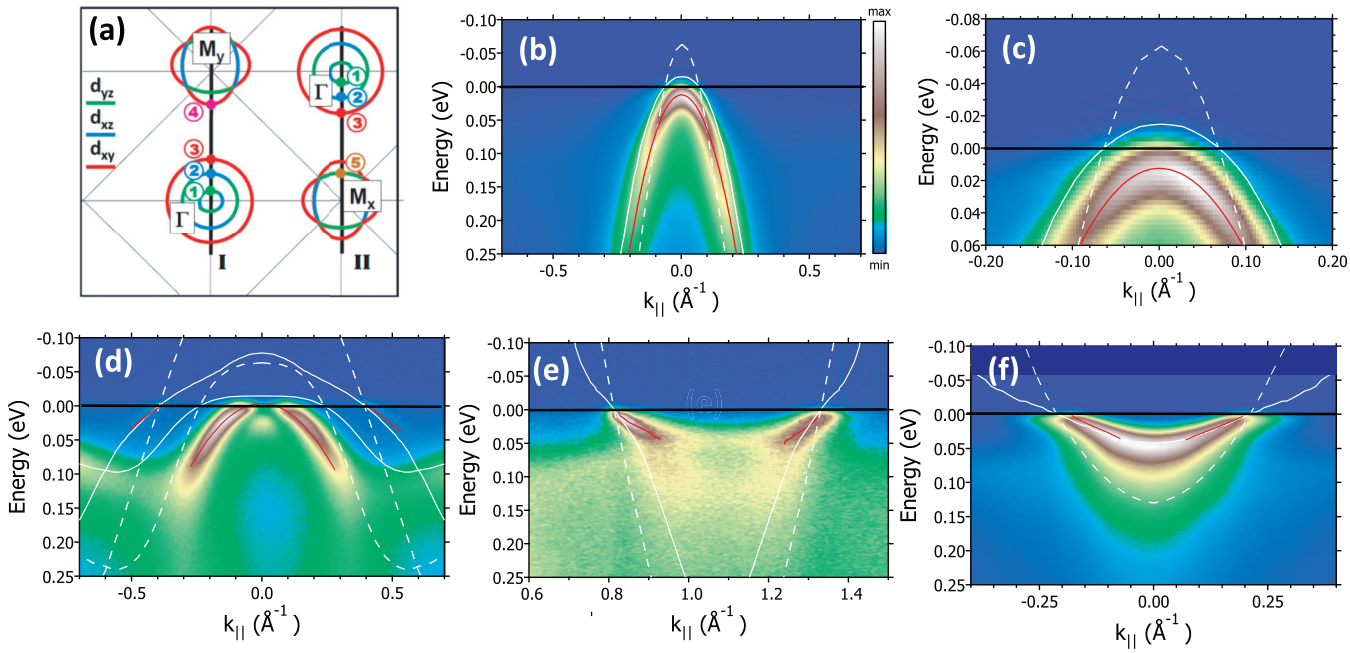

FIG. 1. (a) Schematic Fermi surface of LiFeAs in the $k_z = 0$ plane. Sections with different orbital character are marked by different colors [14,15]. (b)–(f) Energy momentum distribution maps (EMDM) measured at various points indicated in (a). Red lines: dispersions derived from fits of ARPES data. Dashed white lines: dispersions from DFT calculations. Solid white lines: dispersions from DFT+DMFT calculations. (b) Data from the inner hole pocket with d_{yz} orbital character, measured near Γ [point (1)] along cut I with *s*-polarized photons (energy $h\nu = 82$ eV). (c) Zoom into the top of the inner hole pocket. (d) Similar data as in (b) but measured with *p*-polarized light (energy $h\nu = 49$ eV). The outer y[d_{xy} orbital character, point (3)] and the middle [d_{xz} orbital character, point (2)] hole pockets are visible. (e) EMDM measured along cut I near M_y with *s*-polarized photons ($h\nu = 123$ eV) showing the outer electron pocket [d_{xy} orbital character, point (4)]. (f) EMDM measured with *s*-polarized photons ($h\nu = 84$ eV) along cut II showing the electron pocket [d_{yz} orbital character, point (5)] near the M_x point.

Debye energy of ≈0.03 eV [45]. In the case when a band does not cross E_F, e.g., the top of the inner hole pocket is ≈0.012 eV below E_F, the data are limited at low energies. At high energies the data are limited by a finite band width, overlapping bands, or in the case when the spectral weight can no longer be distinguished from the background.

The parameters describing the energy dependence of the inelastic scattering rates (β and γ) are collected in Table I for data corresponding to $k_z = 0$ and $k_z = \pi/c$. In addition we present values of w_0 which are used to subtract the contributions from Γ_e (see Supplemental Material [38]). The error bars are estimated from the analysis of data

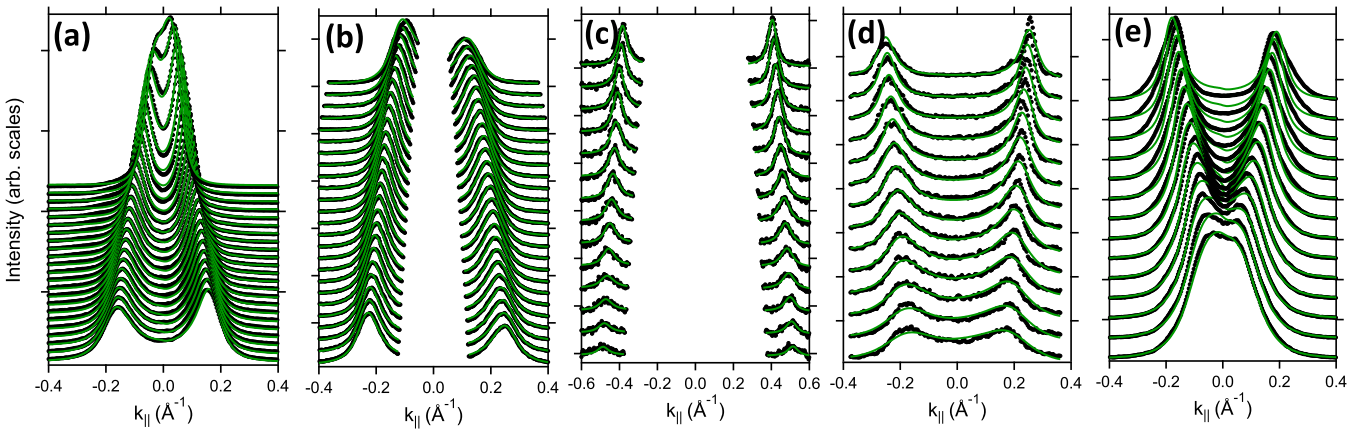

FIG. 2. Waterfall plot of LiFeAs ARPES data (black dots) at 5 points indicated in Fig. 1 (a) together with a fit (green solid lines). (a) Data from point (1). Energy range from 0.15 eV (lowest spectrum) to 0.02 eV (uppermost spectrum). (b) Data from point (2). Energy range from 0.071 eV (lowest spectrum) to 0.013 eV (uppermost spectrum). (c) Data from point (3). Energy range from 0.032 eV (lowest spectrum) to 0.001 eV (uppermost spectrum). (d) Data from point (4). Energy range from 0.046 eV (lowest spectrum) to 0.007 eV (uppermost spectrum). Data from point (5). Energy range from 0.045 eV (lowest spectrum) to 0.006 eV (uppermost spectrum).

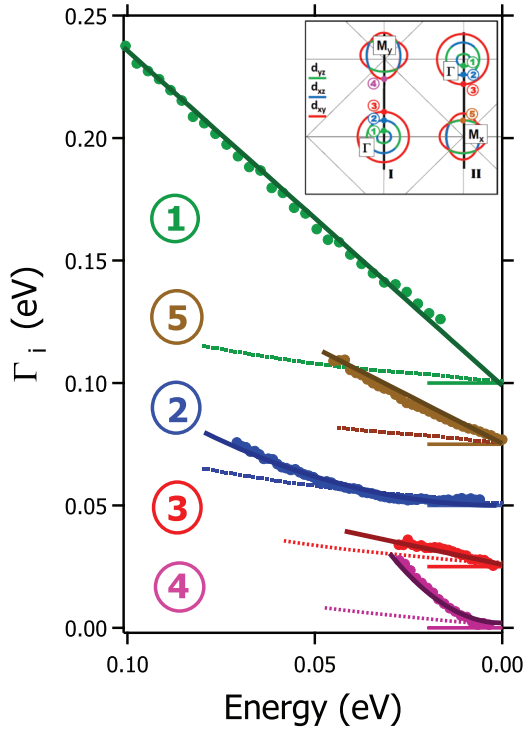

FIG. 3. Insert: the same as Fig. 1(a). Main panel: lifetime broadening Γ_i (large dots) for various points marked in the insert. Solid lines: fit to the data points. Small dots: DFT+DMFT calculations of the scattering rates due to multiorbital electron-electron interactions. The curves are plotted in a stacking mode. The vertical shift between the curves is 0.025 eV. Colors are related to particular sections of the Fermi surface (see inset).

taken at different photon energies and different Brillouin zones.

Moreover we present in Table I the derived mass renormalizations near E_F. These mass renormalizations slightly decrease with increasing binding energy (not shown). Within error bars there is no k_z dependence of all values presented in Table I.

VI. DISCUSSION

Comparing the experimental, the DFT, and the DFT+ DMFT dispersions (see Fig. 1), in all cases the mass renormalization near E_F is well described by DFT+ DMFT calculations. Also no shift between the ARPES data and the DFT+DMFT results is observed at points (3), (4), and (5). However, near $k = 0$ and k_F, shifts of about 0.07 eV to higher energies are observed at points (1) and (2) between the DFT dispersion and the ARPES dispersion. This shift leads to a shrinking or disappearance of the middle and the inner hole pockets on the Fermi surface, respectively. This shift is not reduced near the calculated k_F points by DFT+DMFT calculations (see also Refs. [31,35]).

Regions with a linear increase of the scattering rates as a function of energy have been detected in other FeSCs and related compounds and were discussed in previous publications [44,46–48] in terms of momentum and not orbital dependent strong correlation effects and the proximity to the Planckian limit [49].

Interestingly, the scattering rate at point (1) extrapolates to zero and not to the top of the band at $E_t \approx 0.012$ eV. If hole and electron pockets both cross the Fermi level [see Fig. 4(a)] the phase space for the Augerlike interband transitions goes to zero because of the Pauli principle. If the hole pocket is below E_F at E_t [see Figs. 4(b) and 4(c)], transitions from the hole band to the electron band are only possible when the energy of the interband transition is larger than E_t [see Fig. 4(c)]. Thus at the top of the hole pocket the scattering rate should disappear because, due to the Pauli principle, the phase space for the transitions disappears. This was also discussed for the superconducting case where the scattering rate should go to zero at three times the superconducting gap energy Δ [50].

However, the situation is completely different for a strongly correlated system. There the Fermi edge in momentum space is broadened leading to unoccupied states below the Fermi momentum. Therefore interband transitions into states from the electron pocket below the Fermi level are allowed. The reason for this is that the Pauli principle in this case is no more operative. This leads to a finite phase space for interband transitions even at the top of the hole pocket and therefore to a finite scattering rate. This is illustrated in Fig. 4(d). Thus there is a fundamental difference of the scattering rates between weakly correlated and strongly correlated systems. A similar argumentation was used to explain the enhanced scattering rates at low energies in highly correlated systems leading to the appearance of marginal Fermi liquids [51].

Different from our previous studies on $BaFe_2(As_{1-x}P_x)_2$ and $EuFe_2(As_{1-x}P_x)_2$ [46] in which all energy dependencies of the inelastic scattering rates were assumed to be

TABLE I. ARPES data of LiFeAs derived at various high-symmetry points (HSP) [Fig. 1(a)] for $k_z = 0$ and $k_z = \pi/c$ having predominantly an orbital character OC. m^*/m_b is the mass renormalization. w_0 is the momentum width near E_F caused by elastic scattering. β gives the slope in regions of a linear energy dependence of the scattering rate for points (1), (3), and (5). The parameter γ is related to the quadratic increase of the scattering rates at points (2) and (4). n.a. means not applicable.

HSP	OC	m^*/m_b	w_0(Å^{-1})	β	γ (eV)$^{-1}$	m^*/m_b	w_0(Å^{-1})	β	γ (eV)$^{-1}$
		$k_z = 0$				$k_z = \pi/c$			
(1)	yz	1.6 ± 0.4	0.00 ± 0.01	1.3 ± 0.1	n.a.	n.a.	n.a.	n.a.	n.a.
(2)	xz	1.3 ± 0.5	0.03 ± 0.1	n.a.	5 ± 4	2 ± 0.2	0.03 ± 0.1	n.a.	18 ± 4
(3)	xy	3.9 ± 0.1	0.03 ± 0.01	0.3 ± 0.1	n.a.	3.6 ± 0.1	0.05 ± 0.03	0.7 ± 0.2	n.a
(4)	xy	4.8 ± 0.2	0.05 ± 0.01	n.a.	32 ± 5	3 ± 1	0.01 ± 0.02	n.a.	25 ± 5
(5)	yz	2.3 ± 0.1	0.05 ± 0.01	0.7 ± 0.1	n.a.	1.8 ± 0.1	0.10 ± 0.02	0.6 ± 0.2	n.a.

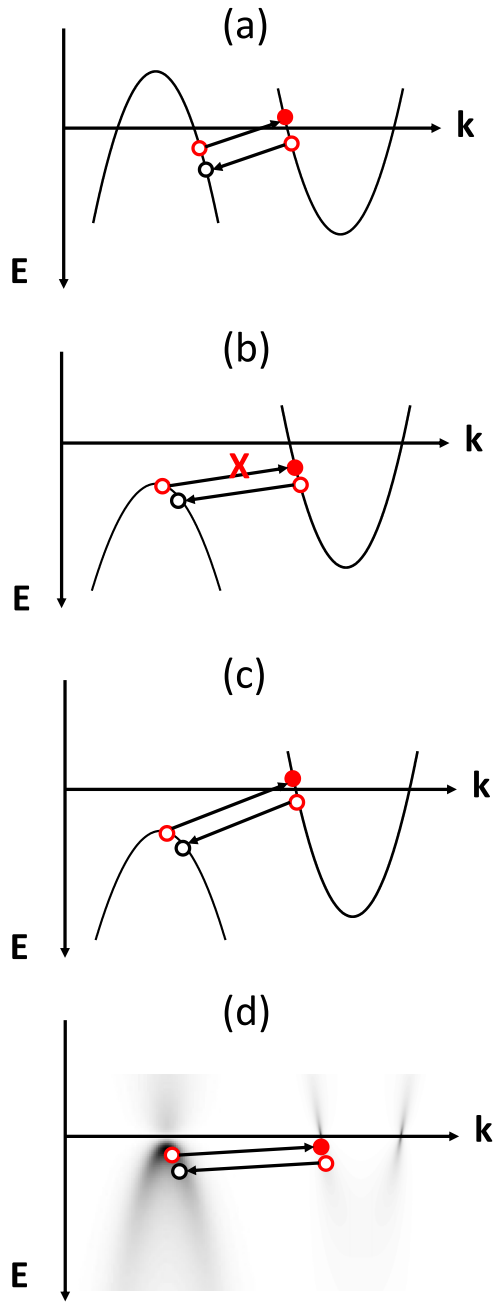

FIG. 4. Relaxation process of a photo hole in a hole pocket due to interband transitions between the hole pocket and an electron pocket. Black empty circle: initial photo hole. Open red (gray) circles: relaxed hole in the hole pocket and hole in the electron pocket. Filled circle: excited electron in the electron pocket. The black and the red (gray) symbols correspond to the initial and the final final state, respectively. (a) Transitions between an ungaped hole pocket and an electron pocket for a weakly correlated Fermi liquid. (b) and (c) Analogous to (a) but for a gaped hole pocket. (d) Analogous to (b) but for a highly correlated system.

linear, we observe in the present investigation for the middle hole pocket and for d_{xy} sections on the electron pockets [point (4)] a Fermi liquid behavior, i.e., a quadratic increase as a function of energy, in agreement with DFT+DMFT: $\Gamma_i = \gamma E^2$ (see Fig. 3). This indicates coherent electronic states at this point at low energies. The prefactor $\gamma \approx 30$ eV^{-1} of this energy dependence at point (4) is very large which leads to a crossover to incoherent states at rather low energies of $\approx$0.03 eV corresponding to room temperature. We contrast the large prefactor $\gamma \approx 30$ eV^{-1} detected at this point with a much smaller prefactor $\gamma \approx 0.28$ eV^{-1} derived for a weakly correlated electronic structure of a Mo surface [37]. Regarding the steep energy dependence, an orbital selective crossover has been detected as a function of temperature in ARPES measurements of FeSCs [26,52,53].

Naively one would expect that because of the connection of $\Re\Sigma$ with $\Im\Sigma$ by the Kramers-Kronig relation, the mass renormalization m^*/m_b would scale with the strength of the scattering rates. Looking at Table I to the data at point (1) and (3) the ratio between m^*/m_b and β is about 0.4 and 3, respectively. Regarding the relationship between Γ, Z, m^*/m_b, and $\Im\Sigma$ presented in the Introduction, a small scattering rate together with a small Z (large m^*/m_b) yields a large $\Im\Sigma$ and thus via the Kramers-Kronig relation a large mass renormalization. This shows that also the data for Γ and m^*/m_b at points (1) and (3) may be compatible with the Kramers-Kronig relation.

We point out that the location of the hot spots coincides with regions where the highest superconducting gaps were detected [24,54]. In particular we mention that the inner yz hole is still important for superconductivity because due to correlation induced broadening of the bands there is still spectral weight at E_F [see Fig. 1(c)]. The reason for this is that the difference between E_F and the maximum of the band ($E_t \approx 0.012$ eV) is smaller than the coupling energies of spin fluctuation (of the order of 0.01 to 0.1 eV [2]) and should therefore, in an Eliashberg model, contribute to the superconducting transition temperature [55]. The present discussion is also important for many other iron-based superconductors, e.g., the ferrochalcogenides, where the top of the hole pockets are very close to E_F.

The observation of Fermi liquid behavior on hole and electron pockets is in line with transport data [56] which derived a Fermi liquid behavior both in hole and electron pockets. Quantum oscillation experiments [57,58] came to the conclusion that the scattering rates for electrons are smaller than those of holes in agreement with the present result. Their derived mass enhancements are comparable to the present results. Regarding the quadratic increase of Γ_i at points (2) and (4) we mention that our data are also consistent with optical spectroscopy data [4,5] because the optical conductivity in a multiorbital system is dominated by cold spots.

VII. CONCLUSIONS

From our ARPES studies of the scattering rates in LiFeAs we conclude that nonlocal effects leading to a momentum dependence of correlation effects are important in these multiorbital compounds. Our results should be contrasted with recent ARPES results of the mass renormalization in Sr_2RuO_4, which do not imply momentum dependent many-body effects [59]. Furthermore, our results indicate that strong electronic fluctuations between hot spots on the hole and electron pockets are important for antiferromagnetism and superconductivity. We also find cold spots on particular sections of the BZ with Fermi liquid behavior which determine the transport and thermal properties.

ACKNOWLEDGMENTS

This work has been supported by the Deutsche Forschungsgemeinschaft (DFG) through the Priority Programme SPP1458, through the Emmy Noether Programm in project WU595/3-3 (S.W.) and through Research Training Group GRK 1621. L.C.'s work is supported by CNPq (Grant No. 304035/2017-3). M.E.'s work is supported by the DFG Project Number GRK 1621.

[1] Y. Kamihara, T. Watanabe, M. Hirano, and H. Hosono, J. Am. Chem. Soc. **130**, 3296 (2008).

[2] D. C. Johnston, Adv. Phys. **59**, 803 (2010).

[3] F. Rullier-Albenque, D. Colson, A. Forget, and H. Alloul, Phys. Rev. Lett. **103**, 057001 (2009).

[4] N. Barisic, D. Wu, M. Dressel, L. J. Li, G. H. Cao, and Z. A. Xu, Phys. Rev. B **82**, 054518 (2010).

[5] A. Tytarenko, Y. Huang, A. de Visser, S. Johnston, and E. van Heumen, Sci. Rep. **5**, 12421 (2015).

[6] I. I. Mazin, D. J. Singh, M. D. Johannes, and M. H. Du, Phys. Rev. Lett. **101**, 057003 (2008).

[7] K. Haule and G. Kotliar, New J. Phys. **11**, 025021 (2009).

[8] M. Aichhorn, L. Pourovskii, V. Vildosola, M. Ferrero, O. Parcollet, T. Miyake, A. Georges, and S. Biermann, Phys. Rev. B **80**, 085101 (2009).

[9] M. Aichhorn, S. Biermann, T. Miyake, A. Georges, and M. Imada, Phys. Rev. B **82**, 064504 (2010).

[10] L. de Medici, Phys. Rev. B **83**, 205112 (2011).

[11] P. Werner, M. Casula, T. Miyake, F. Aryasetiawan, A. J. Millis, and S. Biermann, Nat. Phys. **8**, 331 (2012).

[12] E. Razzoli, C. E. Matt, M. Kobayashi, X.-P. Wang, V. N. Strocov, A. van Roekeghem, S. Biermann, N. C. Plumb, M. Radovic, T. Schmitt, C. Capan, Z. Fisk, P. Richard, H. Ding, P. Aebi, J. Mesot, and M. Shi, Phys. Rev. B **91**, 214502 (2015).

[13] E. Bascones, B. Valenzuela, and M. J. Calderón, C. R. Phys. **17**, 36 (2016).

[14] S. Graser, T. A. Maier, P. J. Hirschfeld, and D. J. Scalapino, New J. Phys. **11**, 025016 (2009).

[15] A. F. Kemper, M. M. Korshunov, T. P. Devereaux, J. N. Fry, H.-P. Cheng, and P. J. Hirschfeld, Phys. Rev. B **83**, 184516 (2011).

[16] A. Damascelli, Z. Hussain, and Z.-X. Shen, Rev. Mod. Phys. **75**, 473 (2003).

[17] G. D. Mahan, *Many-Particle Physics* (Kluwer Academic/ Plenum Publishers, New York, 2000).

[18] J. H. Tapp, Z. Tang, B. Lv, K. Sasmal, B. Lorenz, P. C. W. Chu, and A. M. Guloy, Phys. Rev. B **78**, 060505(R) (2008).

[19] A. Lankau, K. Koepernik, S. Borisenko, V. Zabolotnyy, B. Büchner, J. van den Brink, and H. Eschrig, Phys. Rev. B **82**, 184518 (2010).

[20] V. B. Nascimento, A. Li, D. R. Jayasundara, Y. Xuan, J. O'Neal, S. Pan, T. Y. Chien, B. Hu, X. B. He, G. Li, A. S. Sefat, M. A. McGuire, B. C. Sales, D. Mandrus, M. H. Pan, J. Zhang, R. Jin, and E. W. Plummer, Phys. Rev. Lett. **103**, 076104 (2009).

[21] E. van Heumen, J. Vuorinen, K. Koepernik, F. Massee, Y. Huang, M. Shi, J. Klei, J. Goedkoop, M. Lindroos, J. van den Brink, and M. S. Golden, Phys. Rev. Lett. **106**, 027002 (2011).

[22] S. V. Borisenko, V. B. Zabolotnyy, D. V. Evtushinsky, T. K. Kim, I. V. Morozov, A. N. Yaresko, A. A. Kordyuk, G. Behr, A. Vasiliev, R. Follath, and B. Büchner, Phys. Rev. Lett. **105**, 067002 (2010).

[23] A. A. Kordyuk, V. B. Zabolotnyy, D. V. Evtushinsky, T. K. Kim, I. V. Morozov, M. L. Kulić, R. Follath, G. Behr, B. Büchner, and S. V. Borisenko, Phys. Rev. B **83**, 134513 (2011).

[24] K. Umezawa, Y. Li, H. Miao, K. Nakayama, Z.-H. Liu, P. Richard, T. Sato, J. B. He, D.-M. Wang, G. F. Chen, H. Ding, T. Takahashi, and S.-C. Wang, Phys. Rev. Lett. **108**, 037002 (2012).

[25] G. Lee, H. S. Ji, Y. Kim, C. Kim, K. Haule, G. Kotliar, B. Lee, S. Khim, K. H. Kim, K. S. Kim, K.-S. Kim, and J. H. Shim, Phys. Rev. Lett. **109**, 177001 (2012).

[26] H. Miao, Z. P. Yin, S. F. Wu, J. M. Li, J. Ma, B.-Q. Lv, X. P. Wang, T. Qian, P. Richard, L.-Y. Xing, X.-C. Wang, C. Q. Jin, K. Haule, G. Kotliar, and H. Ding, Phys. Rev. B **94**, 201109(R) (2016).

[27] V. Brouet, D. LeBoeuf, P.-H. Lin, J. Mansart, A. Taleb-Ibrahimi, P. Le Fevre, F. Bertran, A. Forget, and D. Colson, Phys. Rev. B **93**, 085137 (2016).

[28] T. Hajiri, T. Ito, M. Matsunami, B. H. Min, Y. S. Kwon, K. Kuroki, and S. Kimura, Phys. Rev. B **93**, 024503 (2016).

[29] R. P. Day, G. Levy, M. Michiardi, B. Zwartsenberg, M. Zonno, F. Ji, E. Razzoli, F. Boschini, S. Chi, R. Liang, P. K. Das, I. Vobornik, J. Fujii, W. N. Hardy, D. A. Bonn, I. S. Elfimov, and A. Damascelli, Phys. Rev. Lett. **121**, 076401 (2018).

[30] Z. P. Yin, K. Haule, and G. Kotliar, Nat. Mater **10**, 932 (2011).

[31] J. Ferber, K. Foyevtsova, R. Valenti, and H. O. Jeschke, Phys. Rev. B **85**, 094505 (2012).

[32] I. Morozov, A. Boltalin, O. Volkova, A. Vasiliev, O. Kataeva, U. Stockert, M. Abdel-Hafiez, D. Bombor, A. Bachmann, L. Harnagea, M. Fuchs, H.-J. Grafe, G. Behr, R. Klingeler, S. Borisenko, C. Hess, S. Wurmehl, and B. Büchner, Crystal Growth & Design **10**, 4428 (2010).

[33] J. Fink, S. Thirupathaiah, R. Ovsyannikov, H. A. Duerr, R. Follath, Y. Huang, S. de Jong, M. S. Golden, Y.-Z. Zhang, H. O. Jeschke, R. Valenti, C. Felser, S. Dastjani Farahani, M. Rotter, and D. Johrendt, Phys. Rev. B **79**, 155118 (2009).

[34] S. Moser, J. Electron Spectrosc. Relat. Phenom. **214**, 29 (2017).

[35] S. V. Borisenko, D. V. Evtushinsky, Z.-H. Liu, I. Morozov, R. Kappenberger, S. Wurmehl, B. Büchner, A. N. Yaresko, T. K. Kim, M. Hoesch, T. Wolf, and N. D. Zhigadlo, Nat. Phys. **12**, 311 (2015).

[36] G. Grimvall, *The Electron-Phonon Interaction in Metals* (North-Holland, Amsterdam, 1981).

[37] T. Valla, A. V. Fedorov, P. D. Johnson, and S. L. Hulbert, Phys. Rev. Lett. **83**, 2085 (1999).

[38] See Supplemental Material at http://link.aps.org/supplemental/10.1103/PhysRevB.99.245156 providing additional information on the evaluation of scattering rates, which includes Refs. [60–62].

[39] K. Koepernik and H. Eschrig, Phys. Rev. B **59**, 1743 (1999); http://www.fplo.de.
[40] J. P. Perdew, K. Burke, and M. Ernzerhof, Phys. Rev. Lett. **77**, 3865 (1996).
[41] L. Craco, M. S. Laad, S. Leoni, and H. Rosner, Phys. Rev. B **78**, 134511 (2008).
[42] L. Craco and S. Leoni, Sci. Rep. **7**, 46439 (2017).
[43] L. Craco, Phys. Rev. B **77**, 125122 (2008).
[44] J. Fink, E. D. L. Rienks, S. Thirupathaiah, J. Nayak, A. van Roekeghem, S. Biermann, T. Wolf, P. Adelmann, H. S. Jeevan, P. Gegenwart, S. Wurmehl, C. Felser, and B. Büchner, Phys. Rev. B **95**, 144513 (2017).
[45] S. Engelsberg and J. R. Schrieffer, Phys. Rev. **131**, 993 (1963).
[46] J. Fink, A. Charnukha, E. D. L. Rienks, Z. H. Liu, S. Thirupathaiah, I. Avigo, F. Roth, H. S. Jeevan, P. Gegenwart, M. Roslova, I. Morozov, S. Wurmehl, U. Bovensiepen, S. Borisenko, M. Vojta, and B. Büchner, Phys. Rev. B **92**, 201106 (2015).
[47] I. Avigo, S. Thirupathaiah, E. D. L. Rienks, L. Rettig, A. Charnukha, M. Ligges, R. Cortes, J. Nayak, H. S. Jeevan, T. Wolf, Y. Huang, S. Wurmehl, M. I. Sturza, P. Gegenwart, M. S. Golden, L. X. Yang, K. Rossnagel, M. Bauer, B. Büchner, M. Vojta, M. Wolf, C. Felser, J. Fink, and U. Bovensiepen, Phys. Status Solidi B **254**, 1600382 (2017).
[48] J. Nayak, K. Filsinger, G. H. Fecher, S. Chadov, J. Minár, E. D. L. Rienks, B. Büchner, S. P. Parkin, J. Fink, and C. Felser, Proc. Natl. Acad. Sci. USA **114**, 12425 (2017).
[49] J. Zaanen, Nature (London) **430**, 512 (2004).
[50] M. R. Norman and H. Ding, Phys. Rev. B **57**, R11089(R) (1998).
[51] J. Fink, Europhys. Lett. **113**, 27002 (2016).
[52] M. Yi, D. H. Lu, R. Yu, S. C. Riggs, J.-H. Chu, B. Lv, Z. K. Liu, M. Lu, Y.-T. Cui, M. Hashimoto, S.-K. Mo, Z. Hussain, C. W. Chu, I. R. Fisher, Q. Si, and Z.-X. Shen, Phys. Rev. Lett. **110**, 067003 (2013).
[53] M. Yi, Z.-K. Liu, Y. Zhang, R. Yu, J.-X. Zhu, J. J. Lee, R. G. Moore, F. T. Schmitt, W. Li, S. C. Riggs, J.-H. Chu, B. Lv, J. Hu, M. Hashimoto, S.-K. Mo, Z. Hussain, Z. Q. Mao, C. W. Chu, I. R. Fisher, Q. Si, Z.-X. Shen, and D. H. Lu, Nat. Commun. **6**, 7777 (2015).
[54] S. V. Borisenko, V. B. Zabolotnyy, A. A. Kordyuk, D. V. Evtushinsky, T. K. Kim, I. V. Morozov, R. Follath, and B. Büchner, Symmetry **4**, 251 (2012).
[55] W. E. Pickett, Phys. Rev. B **26**, 1186 (1982).
[56] F. Rullier-Albenque, D. Colson, A. Forget, and H. Alloul, Phys. Rev. Lett. **109**, 187005 (2012).
[57] A. I. Coldea, C. M. J. Andrew, J. G. Analytis, R. D. McDonald, A. F. Bangura, J.-H. Chu, I. R. Fisher, and A. Carrington, Phys. Rev. Lett. **103**, 026404 (2009).
[58] C. Putzke, A. I. Coldea, I. Guillamon, D. Vignolles, A. McCollam, D. LeBoeuf, M. D. Watson, I. I. Mazin, S. Kasahara, T. Terashima, T. Shibauchi, Y. Matsuda, and A. Carrington, Phys. Rev. Lett. **108**, 047002 (2012).
[59] A. Tamai, M. Zingl, E. Rozbicki, E. Cappelli, S. Ricco, A. de la Torre, S. McKeown Walker, F. Y. Bruno, P. D. C. King, W. Meevasana, M. Shi, M. Radovic, N. C. Plumb, A. S. Gibbs, A. P. Mackenzie, C. Berthod, H. U. R. Strand, M. Kim, A. Georges, and F. Baumberger, Phys. Rev. X **9**, 021048 (2019) .
[60] S. D. Kevan, Phys. Rev. Lett. **50**, 526 (1983).
[61] J. Tersoff and S. D. Kevan, Phys. Rev. B **28**, 4267 (1983).
[62] A. Herbig, R. Heid, and J. Schmalian, Phys. Rev. B **94**, 094512 (2016).